Chapter 2

Materials and Methodology

2.1 Satellite Data: Key Traits and Attributes

This research utilized a multi-orbiting space platform equipped with both multi-spectral (optical) and microwave (SAR) satellite imagery data. Specifically, the study incorporated Sentinel-1A (C-band) SAR satellite data and optical satellite images from Sentinel-2, sourced from the European Space Agency (ESA).

2.1.1 Optical data images

Optical satellite data captures images within the visible and infrared segments of the electromagnetic spectrum. These images can be presented in natural color, mirroring what is visible to the human eye, or in false color, incorporating both visible and infrared data. False color imagery proves valuable for diverse applications such as agricultural (crop classification), environmental (assessment of vegetation health), and geological (mapping soil composition). Nevertheless, the quality of optical satellite products is susceptible to atmospheric factors, clouds, and rain, hindering precise Earth feature analysis. To overcome these challenges, various atmospheric correction algorithms, including Sen2cor

ATCOR, FLAASH, ACORN, QUAC, and MODTRAN, were employed to enhance optical image quality. This enhancement facilitates a more accurate interpretation of Earth targets. In this thesis, particular emphasis was placed on selecting satellite images acquired on dates with minimal contamination and devoid of clouds. This approach aimed to investigate spectral reflectance responses and derive spectral indices over both vegetation and soil surfaces, ensuring a more robust and reliable analysis.

Sentinel -2 (MSI) satellite data

Launched on June 23, 2015, Sentinel-2 stands as a prominent European Earth Observation (EO) satellite. Sentinel-2 mounts Multi-Spectral Instrument (MSI) which encompasses 13 spectral bands each having different spatial resolutions ranging from 10 to 60-meter pixel size. The Sentinel-2 data underwent image pre-processing in SNAP v 7.0.1, open-source software released under the GNU GPL license-3.0. The reflectance images are derived from Top-of-Atmosphere (TOA) Level 1C, and subsequently processed to Bottom-of-Atmosphere (BOA) Level 2A using the Sen2Cor processor.

With a temporal resolution of 10 days and a radiometric resolution of 12 bits, Sentinel-2 offers a comprehensive observational capability. The spectral specifications of its bands are detailed in Table 2.1. Notably, this satellite plays a pivotal role in Earth observation, providing valuable data for a range of applications, including environmental monitoring, agriculture, and land cover analysis.

2.1.2 SAR satellite data

The utilization of Sentinel-1A SAR satellite imagery played a pivotal role in extracting bio-physical information and retrieving soil moisture through microwave scattering algorithms. Comprehensive specifications for SAR satellite data can be found in Table 2.2. The subsequent subsections provide concise insights into the preprocessing steps applied to SAR

Table 2.1 A detailed illustration of Sentinel-2 MSI Band Specifications.

Spectral Band	Spatial Resolution	Central Wavelength	Bandwidth
B1	60 m	443 nm	21 nm
B2	10 m	490 nm	66 nm
B3	10 m	560 nm	36 nm
B4	10 m	665 nm	31 nm
B5	20 m	705 nm	15 nm
B6	20 m	740 nm	15 nm
B7	20 m	783 nm	20 nm
B8	10 m	842 nm	106 nm
B8a	20 m	865 nm	21 nm
B9	60 m	940 nm	20 nm
B10	60 m	1375 nm	31 nm
B11	20 m	1610 nm	91 nm
B12	20 m	2190 nm	175 nm

data and the computational procedures involved in deriving the backscattering coefficient. This ensures a foundational understanding of the methodologies employed in the study. The procedural framework has been tailored for seamless integration into the Sentinel

Table 2.2 A detailed illustration of Sentinel-1 SAR Specifications.

Property	Details
Launched Date	3 April 2014
Agency	ESA
Frequency	C-band (5.405 GHz)
Polarization	VV + VH
Spatial Resolution	10 m
Temporal Resolution	12 days
Incidence Angle	25° - 43°

application platform (SNAP) tool, an open-source tool made available by the European Space Agency (ESA). The processing graph, presented is written in '.xml' format which enables the command line and framework for the parallel and batch processing of large and extensive satellite datasets. The pre-processing workflow for SAR data is comprised

of several key processing steps strategically organized to minimize error propagation in subsequent stages. These steps are elaborated upon in the subsequent subsections.

Orbit file integration

The metadata file of SAR products includes orbit state vector information for the Sentinel-1 satellite. Precise satellite orbits are determined days to weeks after product generation. Within SNAP software, the activation of a precise orbit option prompts the automatic retrieval and synchronization of orbit state vectors linked to every SAR scene outlined in the product metadata. This process guarantees the acquisition of precise satellite positioning and velocity data, enhancing the overall accuracy of the information gathered.

Removal of thermal noise

Sentinel-1A VH-polarized images contend with thermal noise, notably in the cross-polarization channel. Thermal noise removal is crucial for normalizing backscattering signals and reducing disruptions in multi-swath acquisitions. Level-1 product generation involves correcting sampling start times for Earth's curvature changes.

Calibration

The calibration of the Sentinel-1 SAR satellite involves converting satellite pixel values to radiometrically calibrated SAR backscattering coefficients (σ_0). This calibration process utilizes information contained within the Sentinel-1 GRD product. A calibration vector, provided as an annotation in the product, facilitates a straightforward conversion of image intensity values into σ_0 values. Calibrating the data is readily achievable using the following relations.

$$\sigma_0 = \frac{DN^2}{A_\sigma^2} \tag{2.1}$$

- A_σ is radar cross-section.
- DN represents the Digital Number of the pixel, which, in the case of GRD, corresponds to the pixel amplitude directly extracted from the measurement file.

Speckle noise correction

Speckle noise in SAR images is a grainy interference pattern caused by coherent radar signals. Correction methods, such as speckle filters (e.g., Lee, Frost), multi-looking, and wavelet-based techniques, are employed to mitigate this noise. These approaches aim to balance noise reduction without sacrificing essential image details, enhancing the overall interpretability of SAR imagery for various applications.

Geometric correction

Sentinel-1A SAR data, captured at varying angles, undergo geometric corrections for accurate geocoding. The Range Doppler terrain correction, utilizing a Digital Elevation Model (DEM), addresses topography-induced distortions. Aligning the Coordinate Reference System (CRS) with the UTM zone (Zone 44/45, WGS 84) ensures spatial consistency between Sentinel-1A GRD products and Sentinel-2 MSI data grids.

Conversion to dB

After essential SAR data preprocessing, the pivotal step is the conversion to dB. This process optimizes backscattering intensity visualization, compressing the dynamic range for improved interpretation of surface features. The logarithmic scale used enhances radar signal representation, aiding in further image analysis.

2.2 Ground truth data acquisition

In this study, ground truth data for the years 2020 and 2023 is collected during the Rabi season (December to March) at various crop growth stages. Field observations in the region of interest involved visiting multiple geolocations for in-situ measurements of biophysical and soil parameters, aligning with satellite image acquisition dates. These collected field data contribute to the classification of vegetation and soil in SAR satellite imagery. To ensure precise geolocation during field campaigns, a handheld GPS receiver (Trimble Juno 3B) was employed, providing positional accuracy up to 5 meters in latitude and longitude coordinates.

2.2.1 LAI measurement

In this thesis, LAI measurements were carried out on diverse reference fields of varying sizes, synchronized with SAR data acquisition dates. The main goal of the in-situ measurements is to collect LAI data utilizing the Li-Cor measurement device, ensuring meticulous calibration and avoiding any contamination in the acquired measurements. Each LAI measurement involved taking the mean of three readings for accuracy.

2.2.2 Soil moisture (m_v) and surface roughness measurement

The soil moisture measurement employs the Hydra Go device Figure 2.1(a), operating on battery power and capable of penetrating the soil surface at depths between 3 to 5 centimeters. To ensure precision and minimize errors, an average of 3 to 5 measurements is taken. Evaluating surface roughness involves the plate insertion technique, utilizing a metallic plate measuring one meter in length and 0.7 meters in width, marked with a 1 cm^2 grid Figure 2.1(b). This plate is inserted into the soil until the grid lines imprint the roughness profile onto its surface. Subsequently, the image capturing the soil surface's

roughness profile on the plate is digitized to compute parameters such as Root Mean Square (RMS) variation and correlation length.

(a) (b)

Figure 2.1 Illustartion of measurement of (a) soil moisture through HydraGO device and (b) surface roughness employing plate insertion technique

2.3 Methodology

In Figure 2.2, various modeling scenarios depict Earth's surface scattering mechanisms. This thesis employs both backscattering modeling and polarimetric decomposition methodologies. These approaches enhance our analytical capabilities, allowing for an in-depth investigation into the complex interactions between electromagnetic waves and the Earth's surface.

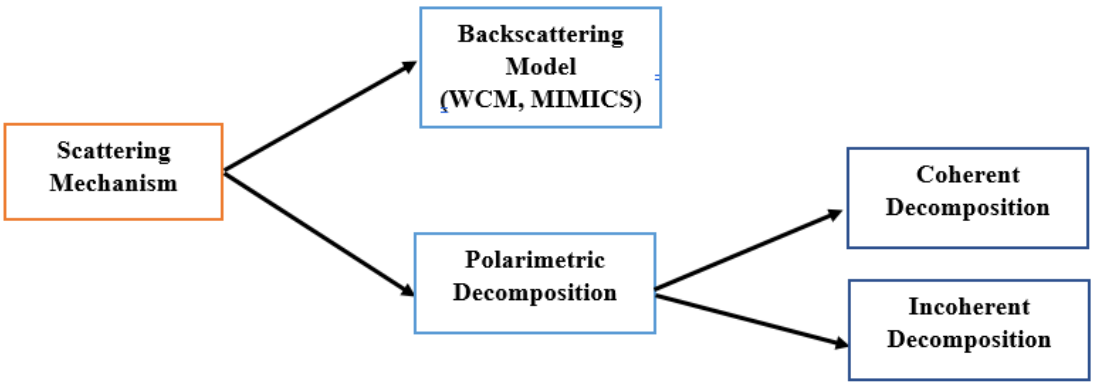

Figure 2.2 Different simulation scenarios for different scattering processes.

2.3.1 Microwave backscattering modelling

In the context of scattering modeling, the comprehensive backscattering response emanating from the Earth's surface is contingent upon a multitude of factors encompassing both sensor properties and Earth target characteristics (Ulaby et al. 1990). The sensor parameters, namely frequency, incidence angle (θ), and polarizations (HH, VV, HV, and VH), constitute integral facets of satellite-borne systems. Concurrently, Earth target parameters, including dielectric constant (ε_s), temperature, orientation, and surface roughness (m_v, s, l), play a pivotal role in shaping the total backscattering response. The sensor parameters aboard satellites are fundamentally central to SAR image processing, exerting substantial influence on the electromagnetic signals returned to the sensor (Karam et al. 1995). It is imperative to recognize that these onboard satellite sensor parameters are characterized by their static and controllable nature. Conversely, Earth target parameters exhibit a highly dynamic profile, serving as dynamic variables responsible for capturing nuanced information pertaining to surface targets on Earth.

In the vegetated covered regions, the total backscattering response (σ^0_T) predominantly comprises contributions stemming from various sources. These contributions can be delineated as (a) Volume Scattering ($\sigma^0_{veg}(V)$), this component emanates from the vegetation canopy itself, encapsulating the scattering effects resulting from the volumetric structure of the vegetation, (b) Surface Scattering ($\sigma^0_{soil}(\varepsilon_s, m_v, \theta)$), originating from the soil surface beneath the vegetation layer, (c) Intermediate Interactions ($\sigma^0_{inter}(\varepsilon_s, m_v, \theta, V)$), this category encompasses interactions occurring between the vegetation canopy and the underlying ground surface. Figure 2.3 shows the different interaction phenomena. The equation form of these components is as follows:

$$\sigma^0_T = \sigma^0_{veg}(V) + \sigma^0_{inter}(\varepsilon_s, m_v, \theta, V) + \tau^2 \sigma^0_{soil}(\varepsilon_s, m_v, \theta) \tag{2.2}$$

where V is the vegetation descriptor used to assess the vegetation condition, $\varepsilon_s, m_v, \theta$ are surface dielectric constant, soil moisture, and incidence angle respectively. $\tau^2 = e^{(-\frac{-2BV}{cos\theta})}$ is two way vegetation attenuation factor. σ^0_{veg} represents backscattered signals from

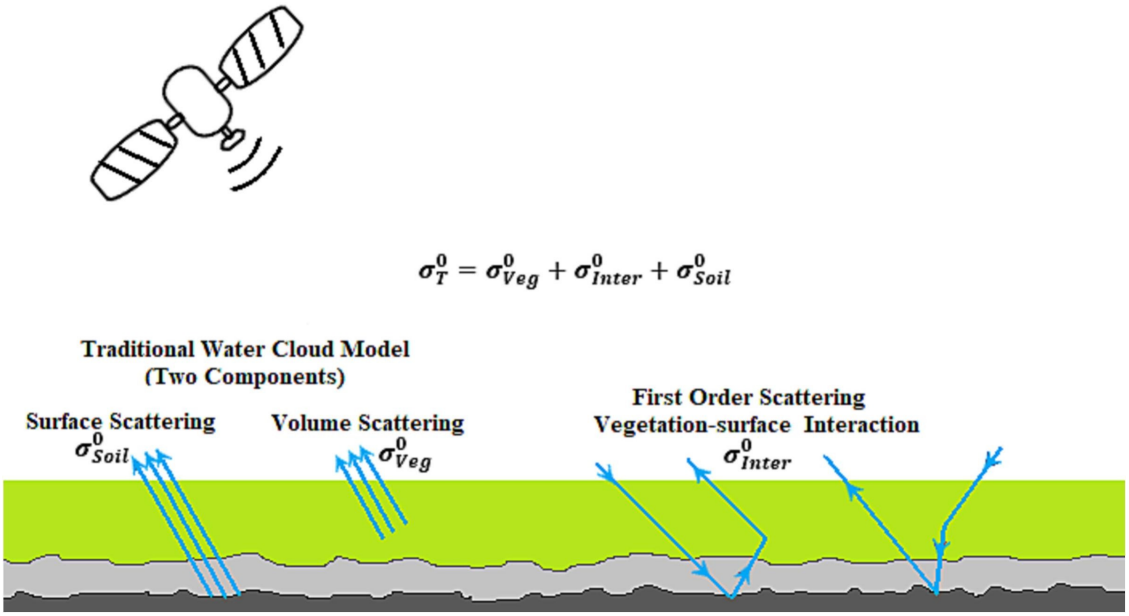

Figure 2.3 Interaction between the radar signal and distinct layers.

vegetation, encompassing volumetric or coherent scattering. Equation 2.3 models this signal, dependent on both sensor parameters and vegetation surface characteristics. The parameters A, E, and B in the model encapsulate contributions from both system-specific and surface-specific factors.

$$\sigma^0_{veg} = AV^E cos\theta \left[1 - e^{-\frac{-2BV}{cos\theta}}\right] \tag{2.3}$$

Furthermore, σ^0_{soil} is delineated as the backscattered echoes originating from the soil surface, encompassing both vegetated and bare soil surfaces. In this thesis, a thorough theoretical examination is undertaken, incorporating an exhaustive analysis of diverse modified geometrical soil scattering and advanced physical soil scattering algorithms. Specifically, the examination includes the integration of prominent models such as the Oh

model, the IEM model, and empirical algorithms, ensuring a comprehensive coverage of soil surface conditions.

2.4 Polarimetric Analysis

In contrast to the WCM which is based on the RTM theory, polarimetric SAR decomposition, an essential principle in PolSAR, emerges as a more pragmatic and streamlined tool for depicting scattering phenomena over agricultural fields. Broadly, divided into two categories of decomposition, the first pertains to coherent target decomposition models, exemplified by the Krogager Decomposition (Krogager et al., 1997) and Cameron Decomposition (Cameron et al., 1996), both reliant on the single-look Sinclair matrix. The second category encompasses incoherent decomposition models, utilizing the multi-look covariance or coherency matrices. Examples of incoherent decomposition include the eigen-based Cloude-Pottier decomposition (Cloude and Pottier, 1997), and model-based Freeman-Durden decomposition (Freeman and Durden, 1998).

Agricultural fields, marked by the dynamic nature of their crop distribution and temporal changes, present as distributed targets with inherent incoherent characteristics. This thesis centers its investigation predominantly on incoherent decomposition methodologies, with a specific emphasis on the Freeman-Durden model-based approach. Within this analytical framework, the scattering process is conceptualized as an incoherent linear summation involving surface, double, and volume scattering models illustrated in Figure 2.4. The Freeman-Durden model, esteemed for its simplicity and intuitive attributes, has exerted a profound influence, serving as a cornerstone for the development of various decomposition methods extensively applied in the extraction of vegetation-related information (An et al., 2010; An et al., 2011; Shan et al., 2012; Trudel et al., 2009; Yamaguchi et al., 2005; Yamaguchi et al., 2006). The scattering matrix contains the polarimetric properties of the target surface. The extraction of information related to scatterers that are pure or

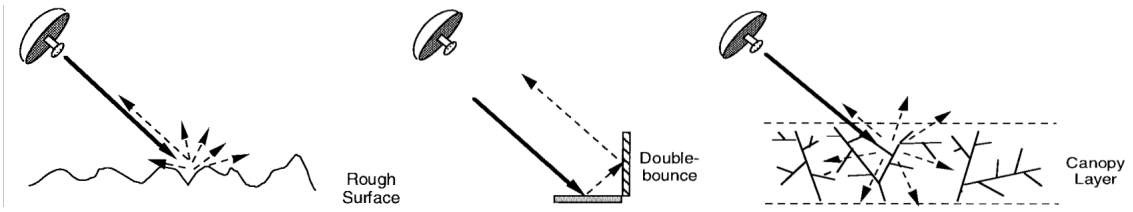

Figure 2.4 Components of scattering in model-based decomposition: Surface scattering (Left), Double-bounce scattering (Middle) and Volume scattering(Right).

isolated may be obtained directly from the scattering matrix. However, when dealing with scatterers that are dispersed, it becomes necessary to use second-order statistics, such as the covariance or coherency matrix, for analysis. The matrices successfully acquire complex information related to the objects being examined.

2.4.1 Scattering, Covariance and Coherency Matrix

When a radar wave encounters a target surface, it experiences a change in its polarization state. The wave that is reradiated from the target surface has responses in both horizontal and vertical polarizations. Within the domain of SAR polarimetry, the reflections originating from the backscattered wave in each polarization channel are recorded and organized in the form of a scattering matrix given by

$$\mathbf{S} = \begin{bmatrix} S_{\mathrm{HH}} & S_{\mathrm{HV}} \\ S_{\mathrm{VH}} & S_{\mathrm{VV}} \end{bmatrix} \tag{2.4}$$

all four elements of the scattering matrix represent the backscattered response of the target within a specific polarization channel. The co-polarized response is in the diagonal signifying that transmitted and received radar waves in the same polarizations. Conversely, the off-diagonal terms signify cross-polarization information, denoting scenarios where the transmitted and received radar waves possess orthogonal polarizations relative to each other.The scattering matrix serves as a means to quantify the data pertaining to an

unaltered object that exhibits a distinct scattering process. However, the characteristics of the Earth often exhibit a complex and widespread nature, displaying a variety of scattering reactions. In these particular situations, the information obtained just from the scattering matrix is insufficient to comprehensively characterize the physical properties of the surface. Therefore, in order to overcome this constraint, it becomes essential to use second-order statistics, such as covariance and coherency matrices. The use of these matrices serves the purpose of acquiring a more thorough comprehension of the intricate scattering characteristics shown by the surface. The matrices discussed in this context are obtained by transforming the scattering matrix into its vectorized version, which is constructed using different bases for example Pauli and Lexicographic bases (Ψ_L) (Navarro-Sanchez et al., 2010). The Lexicographic basis is described as

$$[\Psi_L] = 2\begin{bmatrix} 1 & 0 \\ 0 & 0 \end{bmatrix}, 2\begin{bmatrix} 0 & 1 \\ 0 & 0 \end{bmatrix}, 2\begin{bmatrix} 0 & 0 \\ 1 & 0 \end{bmatrix}, 2\begin{bmatrix} 0 & 0 \\ 0 & 1 \end{bmatrix} \tag{2.5}$$

The vector form obtained by the Lexicographic bases by keeping the reciprocity condition is

$$\mathbf{k} = \begin{bmatrix} S_{HH} \\ \sqrt{2}S_{HV} \\ S_{VV} \end{bmatrix} \tag{2.6}$$

The covariance matrix is defined as $\langle C_3 \rangle = \langle k_L * k_L^{\dagger} \rangle$, for quad polarization case can be written as

$$[\mathbf{C}] = \begin{bmatrix} S_{HH}S_{HH}^* & \sqrt{2}S_{HH}S_{HV}^* & S_{HH}S_{VV} \\ \sqrt{2}S_{HV}S_{HH}^* & 2S_{HV}S_{HV}^* & \sqrt{2}S_{HV}S_{VV}^* \\ S_{VV}S_{HH}^* & \sqrt{2}S_{VV}S_{HV}^* & S_{VV}S_{VV}^* \end{bmatrix} \tag{2.7}$$

For dual polarization case (VV and VH) which is provided by Sentinel-1 imagery, the covariance matrix reduced to $\langle C_2 \rangle$ and can be written as

$$\langle \mathbf{C_2} \rangle = \begin{bmatrix} \langle S_{VV} S_{VV}^* \rangle & \langle S_{VV} S_{VH}^* \rangle \\ \langle S_{VH} S_{VV}^* \rangle & \langle S_{VH} S_{VH}^* \rangle \end{bmatrix} \tag{2.8}$$

Parallel to this, the coherency matrix becomes a complex Hermitian matrix with real elements on its diagonal and complex conjugate entries symmetrically off-diagonal. The naming suggests an instant association with the coherence of the k-vector components. The local fluctuations in scattering phenomena are explained by this matrix. The coherency matrix, a second-order polarimetric descriptor, is constructed from the scattering matrix's vectorized manifestation using Pauli's basis. Pauli matrices are described as follows

$$[\Psi_P] = \sqrt{2} \begin{bmatrix} 1 & 0 \\ 0 & 1 \end{bmatrix}, \sqrt{2} \begin{bmatrix} 1 & 0 \\ 0 & -1 \end{bmatrix}, \sqrt{2} \begin{bmatrix} 0 & 1 \\ 1 & 0 \end{bmatrix}, \sqrt{2} \begin{bmatrix} 0 & -i \\ i & 0 \end{bmatrix} \tag{2.9}$$

The factor $\sqrt{2}$ is used as a normalization constant. The scattering vector obtained from the Pauli matrix basis is given by

$$\mathbf{k_p} = \frac{1}{\sqrt{2}} \begin{bmatrix} S_{HH} + S_{VV} \\ S_{HH} - S_{VV} \\ 2S_{VV} \end{bmatrix} \tag{2.10}$$

The 3×3 Hermitian coherency matrix is obtained from the outer product of k_p, defined as:

$$[\mathbf{T_3}] = \langle k_p . k_p^\dagger \rangle = \tag{2.11}$$

$$\frac{1}{2}\begin{bmatrix} \langle|S_{HH}+S_{VV}|^2\rangle & \langle(S_{HH}+S_{VV})(S_{HH}-S_{VV})^*\rangle & 2\langle(S_{HH}+S_{VV})S_{HV}^*\rangle \\ \langle(S_{HH}-S_{VV})(S_{HH}+S_{VV})^*\rangle & \langle|S_{HH}-S_{VV}|^2\rangle & 2\langle(S_{HH}-S_{VV})S_{HV}^* \\ 2\langle S_{HV}(S_{HH}+S_{VV})^* & 2\langle S_{HV}(S_{HH}-S_{HV})^* & 4\langle|S_{VV}|^2\rangle \end{bmatrix} \tag{2.12}$$

For dual polarized case, the target vector will get reduced to

$$\mathbf{k_p} = \frac{1}{\sqrt{2}}\begin{bmatrix} S_{HH}+S_{VV} \\ S_{HH}-S_{VV} \end{bmatrix} \tag{2.13}$$

or for the Sentinel-1 case, it will be

$$\mathbf{k_p} = \frac{1}{\sqrt{2}}\begin{bmatrix} S_{VV} \\ 2S_{VH} \end{bmatrix} \tag{2.14}$$

From Equation 2.14 the reduced coherency matrix for each pixel can be obtained as:

$$\langle\mathbf{T_2}\rangle = \frac{1}{2}\begin{bmatrix} \langle S_{VV}S_{VV}^*\rangle & \langle 2S_{VV}S_{VH}^*\rangle \\ \langle 2S_{VH}S_{VV}^*\rangle & \langle 4S_{VH}S_{VH}^*\rangle \end{bmatrix} \tag{2.15}$$

2.4.2 Calculation of different polarimetric index

The calculation of different polarimetric indices includes the examination and interpretation of PolSAR data in order to extract significant insights about the underlying surfaces. These indices are often calculated using coherency or covariance matrices, providing valuable information about various scattering processes and physical characteristics of the measured region. The aforementioned indices are of utmost importance in the characterization of

terrain characteristics, the identification of land coverings, and the facilitation of many applications, including vegetation categorization and terrain monitoring.

2.4.3 Degree of Polarization

The degree of polarization (m) quantifies the level of polarization shown by the radar return. The term "signal coherence ratio" denotes the ratio of coherent polarized signals within the overall backscattered radar signal. From Equation 2.8, the calculation of m is as follow:

$$m = \sqrt{1 - \frac{4|C_2|^2}{(Tr(C_2))^2}} \tag{2.16}$$

Using m some of the important indices are derived.

2.4.4 Dual Polarized Radar Vegetation Index (DpRVI)

The DpRVI is one of the most important vegetation indexes which is calculated as:

$$DpRVI = 1 - m * \beta \qquad 0 \leq DpRVI \leq 1 \tag{2.17}$$

the variable β denotes the dominant scattering, determined by calculating the ratio of eigenvalues derived from the covariance matrix, symbolically represented as $\beta = \frac{\lambda_1}{\lambda_1 + \lambda_2}$

2.4.5 Polarimetric radar vegetation index (PRVI)

The PRVI uses a cross-polarized backscattering coefficient and is defined as

$$PRVI = (1 - m) * \sigma^0_{VH} \tag{2.18}$$

2.4.6 Radar vegetation index (RVI)

RVI for Sentinel-1 dual polarization case using σ^0_{VV} and σ^0_{VH} is defined as

$$RVI = \frac{4\sigma^0_{VH}}{\sigma^0_{VV} + \sigma^0_{VH}} \tag{2.19}$$

2.5 Data Fusion

Data fusion is a comprehensive methodology that combines data from several sources or time periods in order to enhance the overall quality of the data, leading to improved analytical results, such as classification or inference (Hall and McMullen, 2004). This procedure involves the integration of data from diverse platforms, such as satellites, airplanes, or ground-based measuring instruments. Multi-sensor data fusion is a distinct aspect of this procedure, which entails the integration of data obtained from disparate sensors such as SAR and optical sensors. Data fusion has substantial impacts in many domains such as remote sensing, military applications, healthcare, and finance. By harnessing data from many sources, it supports improved decision-making, enables more precise predictive modeling, and enhances situational awareness (Pohl and Van Genderen, 1998).

Pixel-level fusion refers to the process of integrating physical factors, such as surface reflectance and radar backscatter, at a granular level. The process of coregistration or geocoding of images is of utmost importance, in addition to the resampling of images to achieve an equivalent pixel size. The aforementioned procedure increases the degree of dimensionality of the data, and further analyses, such as classification, are conducted using the combined data. The process of feature-level fusion involves the extraction or selection of certain characteristics from original pictures, followed by their fusing using statistical techniques. This procedure, akin to pixel-level fusion, involves the modification and transformation of the used data into features that are then used for assessment reasons.

Decision-level fusion refers to the process of evaluating data sources independently, which may entail the use of extracted characteristics. Subsequently, the results obtained from these assessments are combined via the application of decision rules. The objective is to achieve a harmonious alignment of shared results while addressing inconsistencies across various sources.

Furthermore, the methodologies and computational models used in the process of data fusion are subject to ongoing improvement, driven by developments in technology such as machine learning, and deep learning approaches, as well as advancements in sensor technology. These improvements play a significant role in improving the process of integrating diverse data sources, hence increasing its relevance and effectiveness in many fields.

Machine learning techniques, such as artificial neural networks (ANNs) and recurrent neural networks (RNNs), have shown strong skills in effectively processing input that is multi-modal and sourced from several channels. They have exceptional proficiency in autonomously acquiring hierarchical representations and comprehending complicated connections among a wide range of datasets, hence facilitating a more efficient amalgamation of information from many sources.

The incorporation of these sophisticated methodologies in data fusion is of utmost importance owing to their capacity to adjust to diverse data attributes, enhance the process of decision-making, and extract more intricate insights from amalgamated information. The contribution of neural networks in improving feature extraction, pattern recognition, and data representation is of great significance in the advancement of data fusion approaches. This has led to their growing importance in many areas and applications.